Geophysical Research Letters

RESEARCH LETTER
10.1029/2024GL111450

Observations of the Electromagnetic Electron Kelvin-Helmholtz Instability and Its Impact on the Dynamics Inside a Flux Rope

K. Jiang[1], S. Y. Huang[2], Q. M. Lu[3], Z. G. Yuan[1], and Q. Y. Xiong[1]

[1]School of Electronic Information, Hubei Luojia Laboratory, Wuhan University, Wuhan, China, [2]School of Earth and Space Science and Technology, Hubei Luojia Laboratory, Wuhan, China, [3]School of Earth and Space Sciences, University of Science and Technology of China, Hefei, China

Key Points:

- The electromagnetic electron Kelvin-Helmholtz instability (EM EKHI) is identified in a flux rope
- The EM EKHI induces an electron velocity vortex and many small-scale current filaments in the flux rope
- A current filament with strong energy conversion, where reconnection may happen, is found near the electron velocity vortex

Correspondence to:
S. Y. Huang,
shiyonghuang@whu.edu.cn

Citation:
Jiang, K., Huang, S. Y., Lu, Q. M., Yuan, Z. G., & Xiong, Q. Y. (2025). Observations of the electromagnetic electron Kelvin-Helmholtz instability and its impact on the dynamics inside a flux rope. *Geophysical Research Letters*, *52*, e2024GL111450. https://doi.org/10.1029/2024GL111450

Received 17 JUL 2024
Accepted 28 OCT 2024

Abstract The electromagnetic electron Kelvin-Helmholtz instability (EM EKHI) and its impact on the dynamics inside a flux rope (FR) is investigated through observations from the Magnetospheric Multiscale mission. The convection term dominated electric field drives $\boldsymbol{E} \times \boldsymbol{B}$ drift in the FR, which supports a strong electron shear flow. The electron shear flow is unstable to the EM EKHI, which results in an electron velocity vortex and many current filaments in the FR. In one of the current filaments, ion and electron demagnetization and strong energy conversion are observed. The continuous radial nulls and obvious reconstructed X-line topology indicate that magnetic reconnection may occur in this current filament.

Plain Language Summary Magnetic reconnection can release magnetic energy and energize particles. Hence, reconnection is thought to be responsible for many explosive phenomena in space. Flux ropes are generated by reconnection and can affect the reconnection processes in turn. Flux ropes are important places for electron acceleration and energy conversion. However, how these processes happen inside a flux rope is unclear. Using high-resolution data from the Magnetospheric Multiscale mission, we identify electromagnetic electron Kelvin-Helmholtz instability inside a flux rope, which induces an electron velocity vortex and breaks the compact current sheet in the flux rope into many current filaments. A current filament with strong energy conversion is found near the electron velocity vortex. Ions and electrons demagnetization, radial nulls, and reconstructed X-line topology are found inside this current filament, implying that the current filament may be reconnecting. Our observations reveal the complex evolution of a flux rope, which can help to understand the dynamics of flux ropes and the roles of flux ropes playing in the magnetotail.

1. Introduction

Magnetic reconnection, converting energy from the magnetic field to the particles by reconfiguring the topology of the magnetic field, is ubiquitous in the Earth's magnetosphere (Burch et al., 2016; Huang et al., 2018, 2021, 2022; Jiang, Huang, Fu, et al., 2021; Jiang, Huang, Tuan, et al., 2024; Jiang et al., 2019; Lu et al., 2022; Torbert et al., 2018; Zhou et al., 2021).

Flux ropes (FRs), 3D spiral magnetic structures, are important carriers of the magnetic flux and energy released by reconnection (e.g., Huang et al., 2012; Jiang, Huang, Yuan, et al., 2021; Jiang et al., 2023). The generation of FRs can be mainly attributed to two mechanisms. One is the tearing instability in an extended current sheet, which has been verified by simulations and observations (Daughton et al., 2011; Drake et al., 2006; Huang et al., 2016; Wang et al., 2010). Another one is related to the electron Kelvin-Helmholtz instability (EKHI, e.g., Che & Zank, 2020; Fermo et al., 2012). The EKHI includes the electromagnetic electron Kelvin-Helmholtz instability (EM EKHI, e.g., Che & Zank, 2023) and the electrostatic electron Kelvin-Helmholtz instability (ES EKHI), which mainly occurs in the electron diffusion region where the anti-parallel magnetic field is negligible but a high anti-parallel electron velocity shear is present (e.g., Che, 2024). The EM EKHI must couple to the magnetic field, while the ES EKHI must couple to the electric field (e.g., Che, 2024). The EM EKHI is driven by the shear in the electron streams and it is not a direct extension of the ideal magnetohydrodynamics Kelvin-Helmholtz instability (MHD KHI, Che & Zank, 2023). Analytic study shows that the ideal electron frozen-in condition $\boldsymbol{E} + \boldsymbol{v}_e \times \boldsymbol{B} = 0$ must be broken for the occurrence of the EM EHKI, and the growth rate of the EM EKHI is much higher than that of the MHD KHI and the wavelength is much shorter (Che & Zank, 2023). Simulations and observations show that the super-Alfvénic electron shear flow can be formed in the outflow of a reconnection, which is unstable to the EM EKHI (e.g., Huang

et al., 2015; Lu et al., 2023; Zhong et al., 2018). The electron velocity vortex resulting from the EM EKHI will grow and match the magnetic field ultimately (Fermo et al., 2012). Then, reconnection induced by the electron velocity vortex happens, which leads to the generation of FRs (Huang et al., 2015; Zhong et al., 2018). More importantly, the electron velocity vortex induced by the EM EKHI can grow rapidly, which can result in effective electron acceleration (e.g., Che & Zank, 2020; Crawford et al., 2024). Che and Zank (2020) proposed a two-phase electron acceleration mechanism related to the EM EKHI in reconnection (second-order Fermi acceleration): fast-growing multi-vortices generated by EM EKHI can induce stochastic electric fields, which can accelerate electrons to form a power-law energy distribution (e.g., Che & Zank, 2020; Crawford et al., 2024).

FRs are believed to play important roles in the process of reconnection. It is thought that FRs can regulate the reconnection rate (e.g., Karimabadi et al., 2007). By generating secondary FRs, the length of the electron diffusion region can be shortened and the reconnection rate can be enhanced (Daughton et al., 2006). FRs are closely related to the energy conversion processes in reconnection. The coalescence of FRs can lead to reconnection and the dissipation of the magnetic energy (Wang et al., 2016; Zhou et al., 2017). Huang et al. (2019) observed strong energy dissipation without apparent evidence of secondary reconnection inside a FR. They thought that FRs may provide another energy dissipation channel in space (Huang et al., 2019). Furtherly, Wang et al. (2020) gave direct evidence of secondary reconnection inside current filaments inside flux ropes. However, how can reconnection occur inside a FR is elusive. By simulations, Huang et al. (2017) show that the EM EKHI can induce reconnection inside FRs: the EM EKHI triggered by electron shear flow driven by $\boldsymbol{E} \times \boldsymbol{B}$ drift can twist the compact current sheet in the FR and fragment it into many small-scale current filaments. Then, secondary reconnection can occur inside these small current filaments. Finally, the FR will evolve into a turbulent state and electrons can be energized during such a process. However, the simulations have not been justified by *in-situ* observations. In this work, we present an observation of the EM EKHI inside a FR in the Earth's magnetotail, which induces an electron velocity vortex and multiple current filaments. Inside one of the current filaments, a possible reconnection identified by ion and electron demagnetization, strong energy conversion, reliable radial nulls, and reconstructed X-line topology is found.

2. Observations

High-resolution data from the Magnetospheric Multiscale (MMS) mission are used in this work. The Fluxgate Magnetometer (FGM) provides the magnetic field (Russell et al., 2016). The Fast Plasma Investigation (FPI) records the plasma distribution functions and plasma moments (Pollock et al., 2016). The Electric Double Probes (EDP) presents the 3-D electric field (Ergun et al., 2016; Lindqvist et al., 2016). All data are presented in the geocentric solar magnetospheric (GSM) coordinate system and a local boundary normal (LMN) coordinate system.

Figure 1 presents a tailward-moving electron velocity vortex FR reported by Jiang et al. (2023). At ∼ 17:23:30 UT, x components of $\boldsymbol{V_i}$ and $\boldsymbol{V_e}$ change from negative to positive (Figure 1b). Simultaneously, B_z changes from negative to positive (Figure 1a), indicating a tailward-moving X-line. In the tailward outflow region of the reconnection, a FR is observed (as marked by the gray vertical dashed line in Figures 1a and 1b, Jiang et al., 2023). The zoom-in view of the FR in the LMN coordinates is shown in Figures 1c–1i ($\boldsymbol{L}$ = [0.64, −0.77, −0.05], $\boldsymbol{M}$ = [0.64, 0.56, −0.52], $\boldsymbol{N}$ = [0.43, 0.30, 0.85], GSM, Jiang et al., 2023). J_L changes from negative to positive, and J_N changes from positive to negative in the center of the FR (Figure 1d), implying the existence of a flow vortex. The bipolar changes of J_L and J_N are mainly contributed by electrons, thus, it is an electron velocity vortex (as shown by two black vertical dashed lines in Figures 1c–1i, Jiang et al., 2023). The ion flow is steady (Figures 1e and 1f) and is treated as the background flow. V_{eL} and V_{eN} have bipolar changes relative to the background flow, and they are basically consistent with $\boldsymbol{V}_{E\times B}$ (Figures 1e and 1f) in the electron velocity vortex, which means the electron velocity in the electron velocity vortex is mainly supported by $\boldsymbol{E} \times \boldsymbol{B}$ drift. The terms of the generalized Ohm's law are shown in Figures 1g–1i. All components of the electric field have bipolar changes, and they are mainly contributed by the convection term (Figures 1g–1i).

Figure 2 examines the existence of the EM EKHI in the FR and its impact on the dynamics of the FR. The electron velocity relative to the background flow ($\boldsymbol{V_e}$ - $\boldsymbol{V_i}$) is shown in Figures 2c and 2d. Che and Zank (2023) analytically studied the EM EKHI in an inviscid collisionless plasma with a step-function electron shear flow and derived the general dispersion relation and the threshold of the EM EKHI. For a simple but common case where $n_1 = n_2$ and $|B_1| = |B_2|$ (the subscript represents the two sides of the current sheet), which is nearly satisfied in our event (Figures 2a and 2b), the threshold of the EM EKHI (Che & Zank, 2023) is:

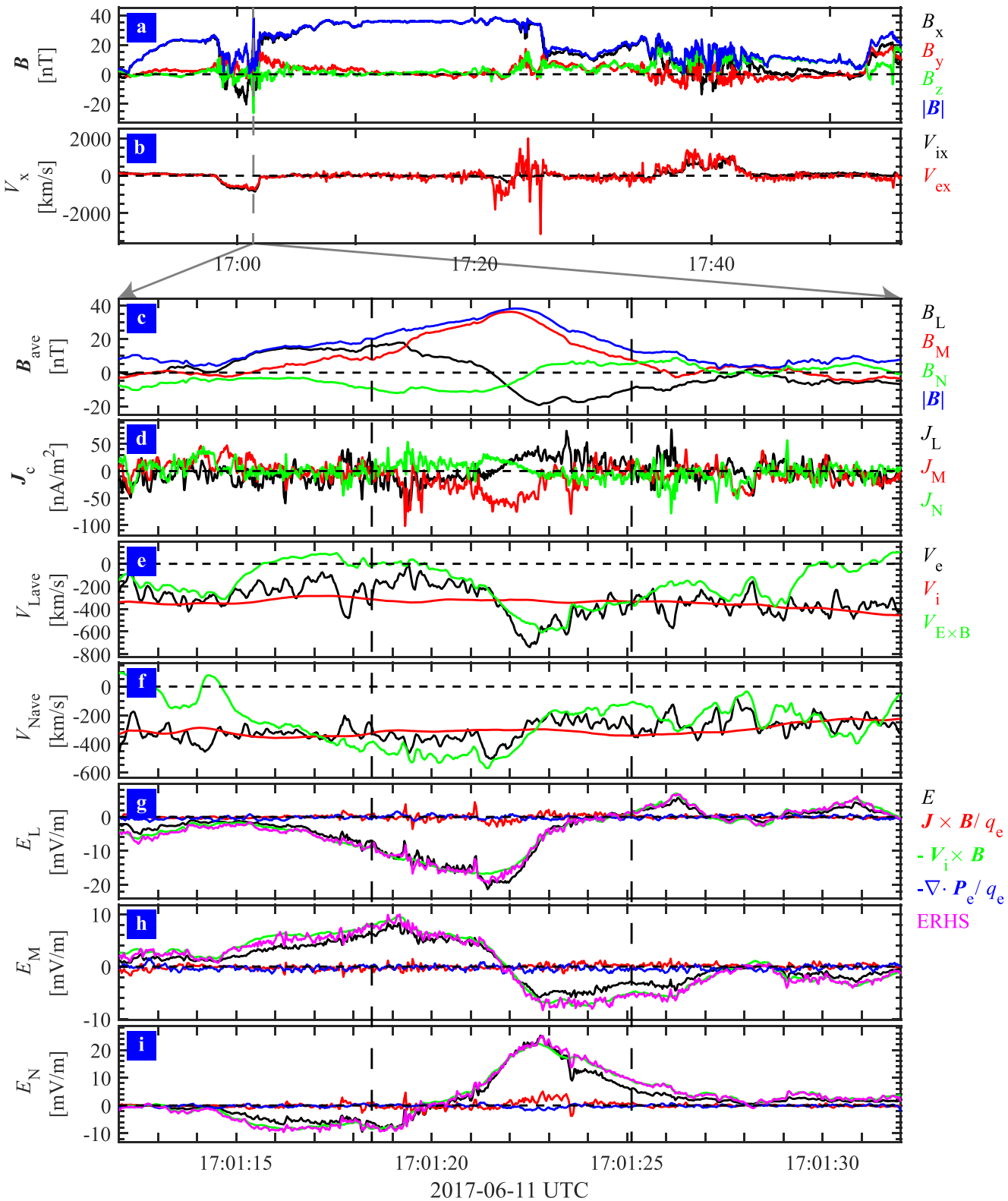
a
b
c
d
e
f
g
h
i
B [nT]
V x [km/s]
B ave [nT]
J c [nA/m2]
V Lave [km/s]
V Nave [km/s]
E L [mV/m]
E M [mV/m]
E N [mV/m]
B x
B y
B z
|B|
V ix
V ex
B L
B M
B N
J L
J M
J N
V e
V i
V E×B
E
J × B/ q e
- V i × B
-∇· P e / q e
ERHS
17:00
17:20
17:40
17:01:15
17:01:20
17:01:25
17:01:30
2017-06-11 UTC

Figure 1.

$$\Delta U > 2|V_{Ae}| \quad (1)$$

where ΔU is the electron velocity shear, and V_{Ae} is the local electron Alfvén speed. V_{eL} and V_{eN} show bipolar changes relative to the background flow in the electron velocity vortex (Figure 2c), but V_{eM} does not (Figure 2d), which means the electron velocity vortex and the electron velocity shear of the electron velocity vortex lie in the LN plane. The reversal points of V_{eL} - V_{iL} and V_{eN} - V_{iN} are not coincident (Figure 2c), which implies that MMS didn't cross the electron velocity vortex along any of the axes of the symmetry of the cross-section of the electron velocity vortex (assuming the shape of the cross-section of the electron velocity vortex is rounded). Thus, we divide the interval of the electron velocity vortex (from 17:01:18.5 to 17:01:25.1 UT) into three parts: the entrance part (from 17:01:18.5 to 17:01:21.6 UT), the center part (from 17:01:21.6 to 17:01:22.4 UT), and the departure part (from 17:01:22.4 to 17:01:25.1 UT), where the center part (from 17:01:21.6 to 17:01:22.4 UT) is from the reversal point of V_{eL} - V_{iL} to the reversal point of V_{eN} - V_{iN}. Then, the maximum velocity shear amplitude is found by subtracting the data points in the entrance part and the departure part points by points. The maximum amplitude of the electron velocity shear is 896 km/s. Then, we project the L and N components of the magnetic field into the direction of the maximum velocity shear and calculate the $2|V_{ae}|$. The maximum velocity shear amplitude (896 km/s, red dashed line in Figure 2e) is much larger than the minimum of $2|V_{ae}|$ in the direction of the maximum velocity shear (79 km/s), indicating that the unstable criterion for the EM EKHI is satisfied within this vortex (Che & Zank, 2023). And the electron velocity vortex in the FR can be induced by the EM EKHI (Che & Zank, 2020; Fermo et al., 2012; Huang et al., 2017; Zhong et al., 2018). An analytical study shows that the ideal electron frozen-in condition must be broken for EM EKHI to occur (Che & Zank, 2023). Simulations show that the electron velocity vortex induced by the EM EKHI is not collocated with the magnetic field at the beginning. As time goes on, the electron velocity vortex will grow and finally coincide with the closed magnetic field lines (e.g., Fermo et al., 2012). Thus, we infer that the electron velocity vortex here is in the later stage of the growth of the EM EKHI, and it partially coincides with the magnetic field. The growth rate of the EM EKHI derived by Che and Zank (2023) are:

$$\gamma_{em} = \frac{1}{n_1 + n_2}\left[n_1 n_2 (\Delta \boldsymbol{U} \cdot \boldsymbol{k})^2 - (n_1 + n_2)\left(n_1 (\boldsymbol{V}_{Ae1} \cdot \boldsymbol{k})^2 + n_2 (\boldsymbol{V}_{Ae2} \cdot \boldsymbol{k})^2\right)\right]^{\frac{1}{2}} \quad (2)$$

where n is the electron density, and k is the wavenumber of the EM EKHI. The electron density and magnitude of the magnetic field are symmetric at two sides of the electron velocity vortex (Figures 2a and 2b). Using $n_1 = n_2 = n_e$ and $|V_{Ae1}| = |V_{Ae2}| = |V_{Ae}|$, the growth rate of the EM EKHI can be rewritten as:

$$\gamma_{em} = \frac{1}{2}\left[(\Delta \boldsymbol{U} \cdot \boldsymbol{k})^2 - (2\boldsymbol{V}_{Ae} \cdot \boldsymbol{k})^2\right]^{\frac{1}{2}} \quad (3)$$

Using the wavenumber of the EM EKHI $\sim 1/d_e$ ($d_e = 4.3$ km is the electron inertial length calculated by the average electron density $n_e = 1.5$ cm^{-3} at two sides of the electron velocity vortex from ~17:01:16 to 17:01:18.5 UT and from ~17:01:25.1 to 17:01:26.4 UT), the maximum amplitude of the electron velocity shear in the LN plane $|\Delta U_{LN}| = 896$ km/s, and the minimum local electron Alfvén velocity along the direction of maximum electron velocity shear $2|V_{AeLN}| = 79$ km/s in the electron velocity vortex, the growth rate of the EM EKHI are estimated as ~104/s. According to the analytic study, the growth rate of the EM EKHI is on the order of the electron gyro-frequency (Che & Zank, 2023). The average local electron gyro-frequency in the electron velocity vortex is 778 Hz (calculated by the average magnitude of the magnetic field 27.8 nT in the electron velocity vortex from 17:01:18.5 to 17:01:25.1 UT). The growth rate of the EM EKHI is comparable to but smaller than the average electron gyro-frequency in the electron velocity vortex, which further supports that the EM EKHI is in the quasi-saturation stage (e.g., Crawford et al., 2024).

Figure 1. Overview of a magnetic reconnection in the magnetotail (a)–(b) and a zoom-in view of the flux rope in the tailward outflow of the reconnection (c)–(i). Data in (a) and (b) are in the survey and fast mode and they are presented in the GSM coordinates; data in (c)–(i) are in the burst mode, and they are displayed in the LMN coordinates. (a) Magnetic field; (b) x components of ion and electron velocity; (c) magnetic field averaged over all MMS; (d) current density calculated by the curlometer method; L (e) and N (f) components of $\boldsymbol{V}_e$, $\boldsymbol{V}_i$, and $\boldsymbol{V}_{E\times B}$ averaged over all MMS; (g)–(i) L, M, and N components of electric field (black), Hall term (red), convection term (green), divergence of electron pressure tensor (blue), and sum (magenta) of Hall term, convection term, and divergence of electron pressure tensor. The gray dashed line in (a)–(b) marks the flux rope, and the black dashed lines in (c)–(i) denote the electron velocity vortex.

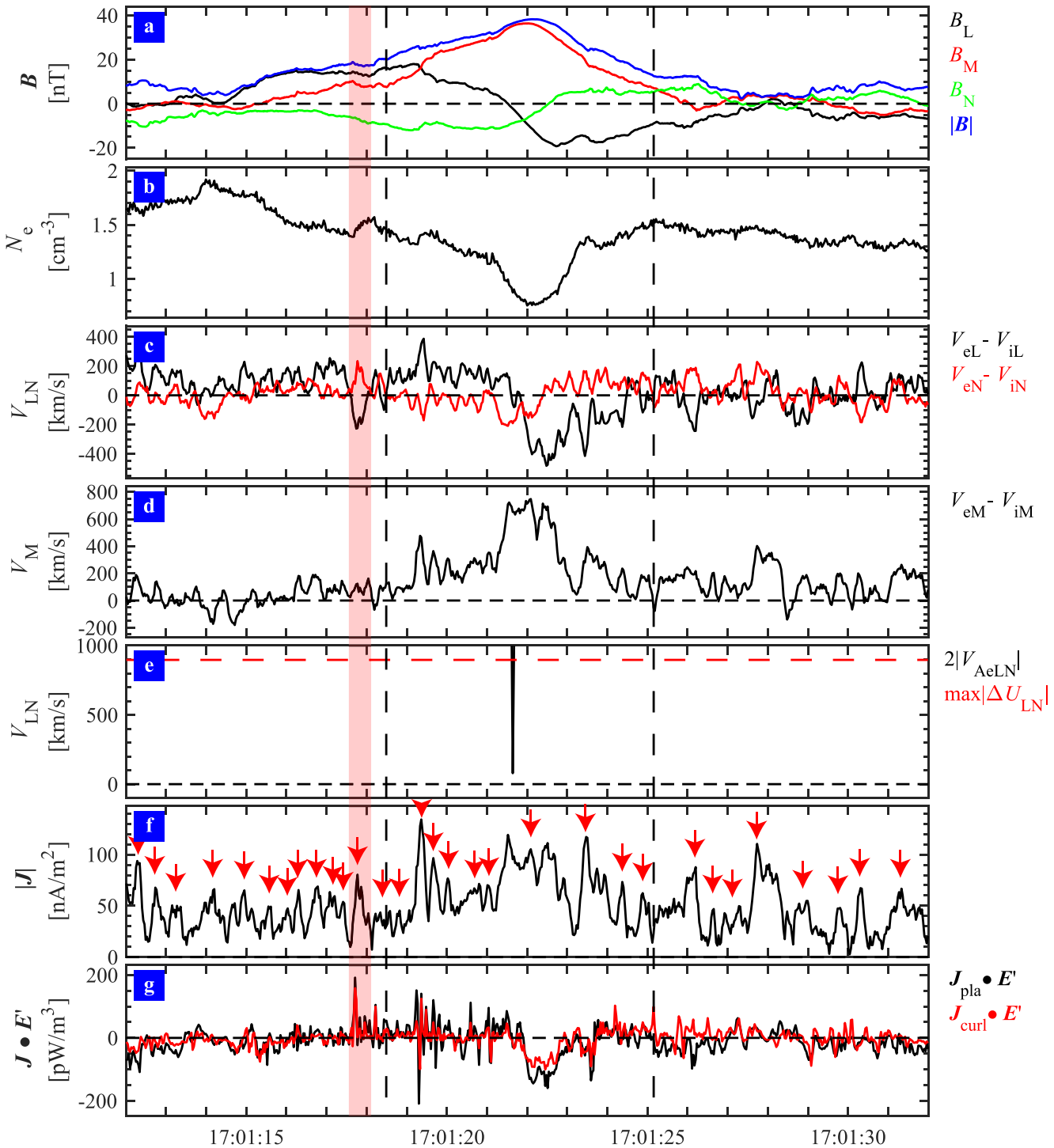

Figure 2. MMS1's observation of the EM EKHI in the flux rope and its impact on the dynamics of the flux rope. (a) Magnetic field; (b) electron density; (c) L and N components of $\boldsymbol{V} = \boldsymbol{V}_e - \boldsymbol{V}_i$; (d) M component of $\boldsymbol{V} = \boldsymbol{V}_e - \boldsymbol{V}_i$; (e) $2|\boldsymbol{V}_{Ae}|$ along the direction of maximum amplitude of the electron velocity shear in the LN plane, the red dashed line is the amplitude of the maximum electron velocity shear in LN plane. (f) The magnitude of current density calculated from plasma moments $\boldsymbol{J} = ne(\boldsymbol{V}_i - \boldsymbol{V}_e)$. The red arrows mark the current filaments. (g) Energy conversion rate $\boldsymbol{J} \bullet \boldsymbol{E}'$, where $\boldsymbol{E}' = \boldsymbol{E} + \boldsymbol{V}_e \times \boldsymbol{B}$ is the electric field in the electron frame, $\boldsymbol{J}_{pla}$ is current density calculated by the plasma moments and $\boldsymbol{J}_{curl}$ is current density calculated by the curlometer method. The black dashed lines in (a)–(g) mark the electron velocity vortex, and the pink shade in (a)–(g) marks the small current filament.

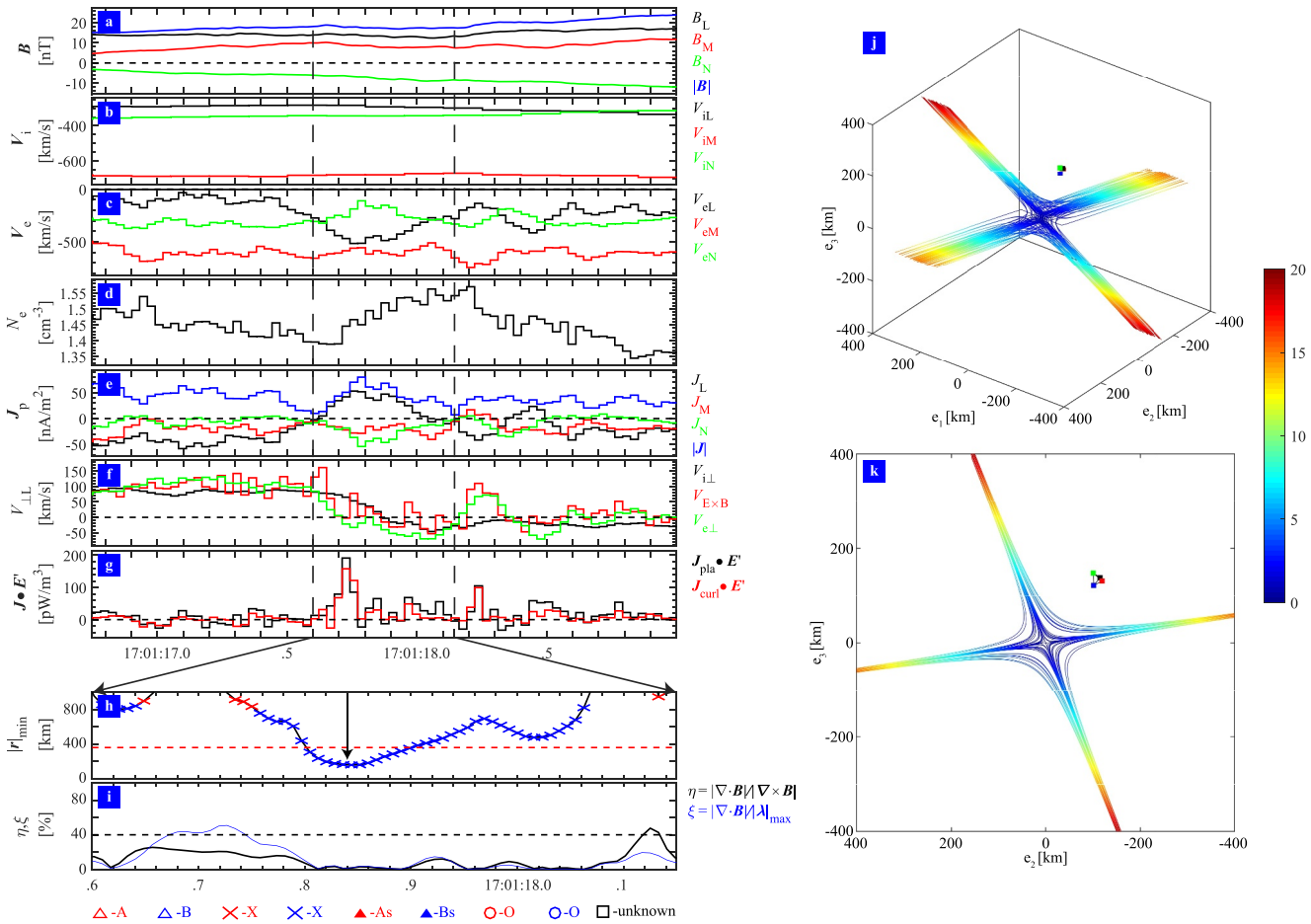

Figure 3. Details of the possible reconnection current filament beside the electron velocity vortex. (a) Magnetic field; (b) $\boldsymbol{V}_i$; (c) $\boldsymbol{V}_e$; (d) electron density; (e) current density calculated by plasma moments; (f) L component of $\boldsymbol{V}_{i\perp}$, $\boldsymbol{V}_{E\times B}$, and $\boldsymbol{V}_{e\perp}$; (g) energy conversion rate; (h) the minimum distance between MMS and magnetic nulls with labels representing different types of the nulls, the horizontal red dashed line is the ion inertial length. The black arrow in (h) marks the time when the magnetic null's topology is reconstructed. (i) $\eta = |\nabla \cdot \boldsymbol{B}|/|\nabla \times \boldsymbol{B}|$ (black line) and $\zeta = |\nabla \cdot \boldsymbol{B}|/|\lambda|_{max}$ (blue line) to quantify the results of the FOTE method, the horizontal black dashed line in (i) is 40%. The symbols at the bottom denote the 3D magnetic nulls (A, B, As, Bs) and the 2D approximation (X and O), the black square is the unknown null. 3D (j) and 2D view (k) of the reconstructed topology of the magnetic null by the FOTE method. Reconstruction is presented in the eigenvector coordinates ($\boldsymbol{e}_1$, $\boldsymbol{e}_2$, $\boldsymbol{e}_3$). The eigenvectors in GSM coordinates are $\boldsymbol{e}_1 = [0.81, -0.07, -0.58]$, $\boldsymbol{e}_2 = [0.06, 0.99, -0.04]$, and $\boldsymbol{e}_3 = [0.58, 0, 0.82]$. The color scale denotes the strength of the magnetic field. The black, red, green, and blue rectangles represent four MMS spacecraft. The black dashed lines in (a)–(g) mark the small current filament.

Plenty of current filaments (as marked by red arrows in Figure 2f) are detected in the FR. It is believed that current filaments can be generated by oblique tearing mode (e.g., Dahlin et al., 2017). However, the tearing mode is not dominant in the flux rope (not shown here). Simulation results show that EM EKHI can twist the compact current sheet in a FR and fragment the compact current sheet into many small-scale current filaments (Huang et al., 2017). Then, secondary reconnection can occur in these current filaments and lead the FR to a turbulent state (Huang et al., 2017). The growth rate of the EM EKHI (on the order of electron gyro-frequency, Che & Zank, 2023) is much faster than that of the tearing instability (on the order of the ion gyro-frequency, Daughton et al., 2011). If the EM EKHI and the tearing mode simultaneously occur in the FR, the EM EKHI will dominate the generation of the current filaments. Thus, the current filaments in the FR should be caused by the EM EKHI. Abundant current filaments imply that the FR is in a turbulent state. A small current filament with strong energy conversion is found near the electron velocity vortex (Figures 2f and 2g, as shown by the pink shade). Inside this current filament, the magnitude of the magnetic field reduces (Figure 2a).

Figure 3 presents the details of the current filament. The duration of the current filament is 0.55 s (from 17:01:17.6–17:01:18.15 UT, as marked by two black vertical dashed lines in Figures 3a–3g). Using the average velocity of the current filament (~478 km/s, not shown here) determined by MDD and STD methods (Shi et al., 2005, 2006), the width of the current filament is estimated as 263 km ~ 0.7 d_i (d_i = 360 km is the ion inertial length calculated by the

average $N_i = 0.4$ cm^{-3} in the lobe region from 17:10 to 17:20 UT). Ion flow does not have a clear change in the current filament (Figure 3b). Thus, the current is mainly contributed by electrons (Figures 3c and 3e). N_e enhances in the current filament (Figure 3d). $\boldsymbol{V}_{i\perp}$ and $\boldsymbol{V}_{e\perp}$ are not consistent with $\boldsymbol{V}_{E\times B}$ (Figure 3f), implying that both ions and electrons are demagnetized. Interestingly, strong energy conversion (up to 191 pW/m^3) is found in the current filament (Figure 3g), which is on the order of the energy conversion of the reported reconnections in the magnetotail (Huang et al., 2018; Jiang, Huang, Wei, et al., 2024; Jiang et al., 2019; Zhou et al., 2019). All these clues imply that magnetic reconnection may happen in this current filament. More convincing evidence supporting that reconnection happens in this current filament is from the results of the First-Order Taylor Expansion (FOTE) method (Fu et al., 2015, 2016). The FOTE method can identify the types of magnetic nulls based on the different combinations of the eigenvalues derived from the Jacobian matrix $\delta\boldsymbol{B}$ and calculate the distance between the magnetic nulls and MMS (Fu et al., 2015). In general, magnetic nulls can be divided into radial nulls (A, B, and X) and spiral nulls (As, Bs, and O), in which A, B, As, and Bs are 3D nulls and X and O are 2D nulls. Two conditions are used to evaluate the reliability of the results of the FOTE method: (a) The minimum distance between the magnetic nulls and the MMS ($|\boldsymbol{r}|_{min}$) should be less than 1 d_i; (b) $\eta = |\nabla\cdot\boldsymbol{B}|/|\nabla\times\boldsymbol{B}|$ and $\zeta = |\nabla\cdot\boldsymbol{B}|/|\lambda|_{max}$ should be less than 40% (Fu et al., 2015). Continuous radial nulls are found by MMS during the crossing of the current filament (Figure 3h). $|\boldsymbol{r}|_{min}$ is less than 1 d_i (ion inertial length is marked by the red horizontal dashed line, Figure 3h) and η and ζ are less than 40% (black horizontal dashed line, Figure 3i) from ~17:01:17.8 to ~17:01:17.9 UT, implying that the radial nulls are reliable (Fu et al., 2015). The 3D topology of the magnetic null (Figure 3j) is reconstructed by the FOTE method at ~17:01:17.84 UT (as marked by the black arrow in Figure 3h), and the 2D projection is shown in Figure 3k. The reconstructed magnetic topologies show a clear X-line configuration, which further backs up that the current filament is reconnecting. One can deduce that MMS was located in the vicinity of the inflow region of the reconnection from the reconstruction (Figures 3j and 3k), which may explain why a reliable LMN coordinates and clear Hall electromagnetic fields cannot be found in this current filament. Besides, the thickness of the current filament may be far less than 0.7 d_i because MMS doesn't traverse the current filament, but crosses the inflow region of the reconnection current sheet. Thus, we deduce that magnetic reconnection occurs in the current filament near the electron velocity vortex induced by the EM EKHI.

3. Discussions and Conclusions

Previous simulations show that the EM EKHI can efficiently twist the magnetic field and generate stochastically distributed and localized inductive electric fields inside the expanding electron velocity vortices (e.g., Che & Zank, 2020). The inductive electric field can efficiently energize electrons and produce the power-law electron energy spectrum (e.g., Che & Zank, 2020; Crawford et al., 2024). The electron velocity vortex lies in the LN plane; thus, the inductive electric field should be along the M direction (e.g., Che & Zank, 2020). According to the Faraday's law and the conservation of the magnetic flux, the inductive electric field caused by the expansion of the electron velocity vortex can be estimated as (e.g., Li et al., 2022):

$$|E| = 2B_0V \tag{4}$$

where B_0 is the average magnitude of the magnetic field in the electron velocity vortex, and V is the expansion speed. We assume that the electron velocity vortex expands at the same velocity as the FR. The velocity of the leading part and the trailing part of the FR estimated by the timing analysis are $V_{TL} = 477\times[-0.61, -0.03, -0.80]$ km/s (LMN) and $V_{TT} = 392\times[-0.34, 0.07, -0.94]$ km/s (LMN), respectively (Jiang et al., 2023). Then, the magnitude of the expansion velocity in the LN plane is 158 km/s. Using the average magnitude of the magnetic field in the electron velocity vortex (27.8 nT) and the expansion velocities, we estimate the inductive electric field as $E_{iM} = 8.8$ mV/m, which is on the same order of E_M in the electron velocity vortex (Figure 1h). However, due to the limited data from MMS, we cannot further evaluate the efficiency of the stochastic electric field from the expansion of the electron velocity vortex in the electron energization.

Using high-resolution data from MMS, we investigated the dynamics of an electron velocity vortex flux rope. The EM EKHI is identified in the flux rope and it is triggered by the electron shear flow supported by $\boldsymbol{E}\times\boldsymbol{B}$ drift. The EM EKHI induces the electron velocity vortex and multiple current filaments in the flux rope. A small-scale current filament is found next to the electron velocity vortex. Inside the current filament, demagnetization of ions and electrons, strong energy conversion, reliable radial nulls, and clear reconstructed X-line topology imply that reconnection may occur inside the current filament, which is consistent with the simulations of Huang

et al. (2017). Our observations can help improve the understanding of the dynamics in the magnetotail, especially the dynamics of the flux ropes.

Data Availability Statement

The MMS data used in this work are publicly available at the MMS Science Data Center (https://lasp.colorado.edu/mms/sdc/public/about/browse-wrapper/).

Acknowledgments
This work was supported by the National Natural Science Foundation of China (42304167, 42074196, 41925018), the Fundamental Research Funds for the Central Universities (2042023kf0097), the China National Postdoctoral Program for Innovative Talents (BX20220238), and the Hubei Provincial Natural Science Foundation of China (2023AFB046). KJ acknowledges the project supported by the Open Fund of Hubei Luojia Laboratory (230100005). We thank the MMS team and instrument leads for data access and support.

References

Burch, J. L., Torbert, R. B., Phan, T. D., Chen, L. J., Moore, T. E., Ergun, R. E., et al. (2016). Electron-scale measurements of magnetic reconnection in space. *Science*, *352*(6290), aaf2939. https://doi.org/10.1126/science.aaf2939

Che, H. (2024). Plasma compressibility and the generation of electrostatic electron Kelvin-Helmholtz instability. *Physics of Plasmas*, *31*(7). https://doi.org/10.1063/5.0208134

Che, H., & Zank, G. P. (2020). Electron acceleration from expanding magnetic vortices during reconnection with a guide field. *The Astrophysical Journal*, *889*(1), 11. https://doi.org/10.3847/1538-4357/ab5d3b

Che, H., & Zank, G. P. (2023). Electromagnetic electron Kelvin-Helmholtz instability. *Physics of Plasmas*, *30*(6). https://doi.org/10.1063/5.0150895

Crawford, C., Che, H., & Benz, A. O. (2024). The scaling of vortical electron acceleration in Thin-current magnetic reconnection and its Implications in solar Flares. *The Astrophysical Journal*, *961*(1), 25. https://doi.org/10.3847/1538-4357/ad09e6

Dahlin, J. T., Drake, J. F., & Swisdak, M. (2017). The role of three-dimensional transport in driving enhanced electron acceleration during magnetic reconnection. *Physics of Plasmas*, *24*(9). https://doi.org/10.1063/1.4986211

Daughton, W., Roytershteyn, V., Karimabadi, H., Yin, L., Albright, B. J., Bergen, B., & Bowers, K. J. (2011). Role of electron physics in the development of turbulent magnetic reconnection in collisionless plasmas. *Nature Physics*, *7*(7), 539–542. https://doi.org/10.1038/Nphys1965

Daughton, W., Scudder, J., & Karimabadi, H. (2006). Fully kinetic simulations of undriven magnetic reconnection with open boundary conditions. *Physics of Plasmas*, *13*(7). https://doi.org/10.1063/1.2218817

Drake, J. F., Swisdak, M., Schoeffler, K. M., Rogers, B. N., & Kobayashi, S. (2006). Formation of secondary islands during magnetic reconnection. *Geophysical Research Letters*, *33*(13). https://doi.org/10.1029/2006gl025957

Ergun, R. E., Tucker, S., Westfall, J., Goodrich, K. A., Malaspina, D. M., Summers, D., et al. (2016). The axial double probe and fields signal processing for the MMS mission. *Space Science Reviews*, *199*(1–4), 167–188. https://doi.org/10.1007/s11214-014-0115-x

Fermo, R. L., Drake, J. F., & Swisdak, M. (2012). Secondary magnetic islands generated by the Kelvin-Helmholtz instability in a reconnecting current sheet. *Physical Review Letters*, *108*(25), 255005. https://doi.org/10.1103/PhysRevLett.108.255005

Fu, H. S., Cao, J. B., Vaivads, A., Khotyaintsev, Y. V., Andre, M., Dunlop, M., et al. (2016). Identifying magnetic reconnection events using the FOTE method. *Journal of Geophysical Research-Space Physics*, *121*(2), 1263–1272. https://doi.org/10.1002/2015ja021701

Fu, H. S., Vaivads, A., Khotyaintsev, Y. V., Olshevsky, V., André, M., Cao, J. B., et al. (2015). How to find magnetic nulls and reconstruct field topology with MMS data? *Journal of Geophysical Research: Space Physics*, *120*(5), 3758–3782. https://doi.org/10.1002/2015ja021082

Huang, C., Lu, Q. M., Guo, F., Wu, M. Y., Du, A. M., & Wang, S. (2015). Magnetic islands formed due to the Kelvin-Helmholtz instability in the outflow region of collisionless magnetic reconnection. *Geophysical Research Letters*, *42*(18), 7282–7286. https://doi.org/10.1002/2015gl065690

Huang, C., Lu, Q. M., Wang, R. S., Guo, F., Wu, M. Y., Lu, S., & Wang, S. (2017). Development of turbulent magnetic reconnection in a magnetic island. *The Astrophysical Journal*, *835*(2), 245. https://doi.org/10.3847/1538-4357/835/2/245

Huang, S. Y., Jiang, K., Yuan, Z. G., Sahraoui, F., He, L. H., Zhou, M., et al. (2018). Observations of the electron jet generated by secondary reconnection in the terrestrial magnetotail. *The Astrophysical Journal*, *862*(2), 144. https://doi.org/10.3847/1538-4357/aacd4c

Huang, S. Y., Jiang, K., Yuan, Z. G., Zhou, M., Sahraoui, F., Fu, H. S., et al. (2019). Observations of flux ropes with strong energy dissipation in the magnetotail. *Geophysical Research Letters*, *46*(2), 580–589. https://doi.org/10.1029/2018gl081099

Huang, S. Y., Retino, A., Phan, T. D., Daughton, W., Vaivads, A., Karimabadi, H., et al. (2016). In situ observations of flux rope at the separatrix region of magnetic reconnection. *Journal of Geophysical Research-Space Physics*, *121*(1), 205–213. https://doi.org/10.1002/2015ja021468

Huang, S. Y., Vaivads, A., Khotyaintsev, Y. V., Zhou, M., Fu, H. S., Retino, A., et al. (2012). Electron acceleration in the reconnection diffusion region: Cluster observations. *Geophysical Research Letters*, *39*(11). https://doi.org/10.1029/2012gl051946

Huang, S. Y., Xiong, Q. Y., Song, L. F., Nan, J., Yuan, Z. G., Jiang, K., et al. (2021). Electron-only reconnection in an ion-scale current sheet at the magnetopause. *The Astrophysical Journal*, *922*(1), 54. https://doi.org/10.3847/1538-4357/ac2668

Huang, S. Y., Zhang, J., Yuan, Z. G., Jiang, K., Wei, Y. Y., Xu, S. B., et al. (2022). Intermittent dissipation at kinetic scales in the turbulent reconnection outflow. *Geophysical Research Letters*, *49*(1), e2021GL096403. https://doi.org/10.1029/2021GL096403

Jiang, K., Huang, S. Y., Fu, H. S., Yuan, Z. G., Deng, X. H., Wang, Z., et al. (2021). Observational evidence of magnetic reconnection in the terrestrial foreshock region. *The Astrophysical Journal*, *922*(1), 56. https://doi.org/10.3847/1538-4357/ac2500

Jiang, K., Huang, S. Y., Wei, Y. Y., Yuan, Z. G., Xiong, Q. Y., Xu, S. B., & Zhang, J. (2024). In situ observations of magnetic reconnection caused by the interactions of two dipolarization fronts. *Geophysical Research Letters*, *51*(12), e2024GL109685. https://doi.org/10.1029/2024gl109685

Jiang, K., Huang, S. Y., Yuan, Z. G., Deng, X. H., Wei, Y. Y., Xiong, Q. Y., et al. (2021). Statistical properties of current, energy conversion, and electron acceleration in flux ropes in the terrestrial magnetotail. *Geophysical Research Letters*, *48*(11). https://doi.org/10.1029/2021GL093458

Jiang, K., Huang, S. Y., Yuan, Z. G., Sahraoui, F., Deng, X. H., Yu, X. D., et al. (2019). The role of upper hybrid waves in the magnetotail reconnection electron diffusion region. *The Astrophysical Journal Letters*, *881*(2), L28. https://doi.org/10.3847/2041-8213/ab36b9

Jiang, K., Huang, S. Y., Yuan, Z. G., Xiong, Q. Y., & Wei, Y. Y. (2023). Observations of tilted electron vortex flux rope in the magnetic reconnection tailward outflow region. *Geophysical Research Letters*, *50*(17), e2023GL105006. https://doi.org/10.1029/2023GL105006

Jiang, K., Huang, S. Y., Yuan, Z. G., Xiong, Q. Y., Xu, S. B., & Lin, R. T. (2024). Observations of energy conversion caused by magnetic reconnection at a dipolarization front. *Geophysical Research Letters*, *51*(6), e2023GL107919. https://doi.org/10.1029/2023gl107919

Karimabadi, H., Daughton, W., & Scudder, J. (2007). Multi-scale structure of the electron diffusion region. *Geophysical Research Letters*, *34*(13). https://doi.org/10.1029/2007gl030306

Li, X. M., Wang, R. S., Lu, Q. M., Russell, C. T., Lu, S., Cohen, I. J., et al. (2022). Three-dimensional network of filamentary currents and superthermal electrons during magnetotail magnetic reconnection. *Nature Communications*, *13*(1), 3241. https://doi.org/10.1038/s41467-022-31025-9

Lindqvist, P. A., Olsson, G., Torbert, R. B., King, B., Granoff, M., Rau, D., et al. (2016). The spin-plane double probe electric field instrument for MMS. *Space Science Reviews*, *199*(1–4), 137–165. https://doi.org/10.1007/s11214-014-0116-9

Lu, Q. M., Fu, H. S., Wang, R. S., & Lu, S. (2022). Collisionless magnetic reconnection in the magnetosphere. *Chinese Physics B*, *31*(8), 89401–089401. https://doi.org/10.1088/1674-1056/ac76ab

Lu, Q. M., Huang, K., Guan, Y. D., Lu, S., & Wang, R. S. (2023). Energy dissipation in magnetic islands formed during magnetic reconnection. *The Astrophysical Journal*, *954*(2), 146. https://doi.org/10.3847/1538-4357/acea86

Pollock, C., Moore, T., Jacques, A., Burch, J., Gliese, U., Saito, Y., et al. (2016). Fast plasma investigation for magnetospheric multiscale. *Space Science Reviews*, *199*(1–4), 331–406. https://doi.org/10.1007/s11214-016-0245-4

Russell, C. T., Anderson, B. J., Baumjohann, W., Bromund, K. R., Dearborn, D., Fischer, D., et al. (2016). The magnetospheric multiscale magnetometers. *Space Science Reviews*, *199*(1–4), 189–256. https://doi.org/10.1007/s11214-014-0057-3

Shi, Q. Q., Shen, C., Dunlop, M. W., Pu, Z. Y., Zong, Q. G., Liu, Z. X., et al. (2006). Motion of observed structures calculated from multi-point magnetic field measurements: Application to cluster. *Geophysical Research Letters*, *33*(8). https://doi.org/10.1029/2005gl025073

Shi, Q. Q., Shen, C., Pu, Z. Y., Dunlop, M. W., Zong, Q. G., Zhang, H., et al. (2005). Dimensional analysis of observed structures using multipoint magnetic field measurements: Application to Cluster. *Geophysical Research Letters*, *32*(12). https://doi.org/10.1029/2005gl022454

Torbert, R. B., Burch, J. L., Phan, T. D., Hesse, M., Argall, M. R., Shuster, J., et al. (2018). Electron-scale dynamics of the diffusion region during symmetric magnetic reconnection in space. *Science*, *362*(6421), 1391–1395. https://doi.org/10.1126/science.aat2998

Wang, R., Lu, Q., Du, A., & Wang, S. (2010). In situ observations of a secondary magnetic island in an ion diffusion region and associated energetic electrons. *Physical Review Letters*, *104*(17), 175003. https://doi.org/10.1103/PhysRevLett.104.175003

Wang, R. S., Lu, Q. M., Nakamura, R., Huang, C., Du, A. M., Guo, F., et al. (2016). Coalescence of magnetic flux ropes in the ion diffusion region of magnetic reconnection. *Nature Physics*, *12*(3), 263–267. https://doi.org/10.1038/Nphys3578

Wang, S., Wang, R., Lu, Q., Fu, H., & Wang, S. (2020). Direct evidence of secondary reconnection inside filamentary currents of magnetic flux ropes during magnetic reconnection. *Nature Communications*, *11*(1), 3964. https://doi.org/10.1038/s41467-020-17803-3

Zhong, Z. H., Tang, R. X., Zhou, M., Deng, X. H., Pang, Y., Paterson, W. R., et al. (2018). Evidence for secondary flux rope generated by the electron Kelvin-Helmholtz instability in a magnetic reconnection diffusion region. *Physical Review Letters*, *120*(7), 075101. https://doi.org/10.1103/PhysRevLett.120.075101

Zhou, M., Berchem, J., Walker, R. J., El-Alaoui, M., Deng, X., Cazzola, E., et al. (2017). Coalescence of macroscopic flux ropes at the subsolar magnetopause: Magnetospheric multiscale observations. *Physical Review Letters*, *119*(5), 055101. https://doi.org/10.1103/PhysRevLett.119.055101

Zhou, M., Deng, X. H., Zhong, Z. H., Pang, Y., Tang, R. X., El-Alaoui, M., et al. (2019). Observations of an electron diffusion region in symmetric reconnection with weak guide field. *The Astrophysical Journal*, *870*(1), 34. https://doi.org/10.3847/1538-4357/aaf16f

Zhou, M., Man, H. Y., Deng, X. H., Pang, Y., Khotyaintsev, Y., Lapenta, G., et al. (2021). Observations of secondary magnetic reconnection in the turbulent reconnection outflow. *Geophysical Research Letters*, *48*(4). https://doi.org/10.1029/2020GL091215